Nuclear Engineering and Technology 56 (2024) 1762–1776

Contents lists available at ScienceDirect

Nuclear Engineering and Technology

journal homepage: www.elsevier.com/locate/net

Original Article

Development and validation of isotope prediction module for VVER spent nuclear fuel analysis

Jaerim Jang [a], Deokjung Lee [b,c,*]

[a] Advanced Reactor Technology Development Division, Korea Atomic Energy Research Institute, Daedeok-daero 989-111, Yuseong-gu, Daejeon, 305-335, Republic of Korea
[b] Department of Nuclear Engineering, Ulsan National Institute of Science and Technology, 50 UNIST-gil, Eonyang-eup, Ulju-gun, Ulsan, 44919, Republic of Korea
[c] Advanced Nuclear Technology and Services, 406-21 Jonga-ro, Jung-gu, Ulsan, 44429, Republic of Korea

ARTICLE INFO

Keywords:
Back-end cycle analysis
Spent nuclear fuel
VVER
Novovoronezh-4
Burnup credit

ABSTRACT

A spent nuclear fuel (SNF) analysis module for the Vodo-Vodyanoi Energetichesky Reactor (VVER) was developed and validated in this study. This advancement expands the application area of the existing nodal diffusion code, RAST-V, and reduces the need for additional code during 3D core simulations for SNF analysis, leading to increased efficiency in simulation time. RAST-V uses Lagrange interpolation and a power correction factor derived from the Bateman equation to bypass the re-depletion calculations, which are used to solve the micro-depletion chain. This approach improved the efficiency of analysis. To mirror the conditions during the 3D core simulations, the module used history indices related to the moderator temperature, fuel temperature, and boron concentration. The module can predict 1620 isotopes. This paper presents the validation of this isotope inventory prediction and the application of burnup credit. The VVER analysis module was validated using 28 samples discharged from the Novovoronezh-4. Most isotopes were within 10 % of the boundaries of the measurements. This study successfully offers verification results using VVER benchmarks and discusses the application of burnup credit using a VVER-440 cask.

1. Introduction

This paper presents a newly developed isotope prediction module for the Vodo-Vodyanoi Energetichesky Reactor (VVER) and its application in spent nuclear fuel (SNF) analysis using various benchmarks and the application of burnup credit through RAST-V for back-end cycle analysis. The SNF analysis module has been implemented in RAST-K for pressurized water reactor (PWR) analysis composed of square type fuel assembly (FA), and the module has been verified and validated (V&V) using 116 SNF benchmarks in previous studies [1–3], showing good agreement with measurements: most isotopes showed a difference within ±5 % [2].

To extend the application area, a VVER analysis module was implemented in RAST-K VVER (RAST-V). VVER is a hexagonal structured PWR, controlled by the Joint Stock Company 'Concern Rosenergoatom' [4,5]. This study assessed the calculation capability of the SNF analysis module for VVER by conducting V&V using two different benchmarks, namely the Novovoronezh Nuclear Power Plant (NPP) Unit 4 [6] and X2 reactor [7]. Specifically, Sample ID 21, discharged from Novovoronezh Unit 4, was used for V&V in a previous study, and it demonstrated comparable accuracy with measurements, achieving ±1σ measurement difference for most isotopes [8]. In previous studies [1,2], Verification and Validation (V&V) were performed using 116 benchmark problems. Among these, 58 benchmarks specifically focused on V&V for predicting isotope inventory and calculating source terms, such as decay heat. The observed differences in the decay heat comparisons were within ±4.3 %, with the prediction of isotope composition for most actinides showing a variance of ±5 %. To evaluate the computational capabilities of the SNF analysis module for VVER Fuel Assemblies (FAs), various benchmarks were employed. A detailed comparison of these benchmarks is presented in Sections 3 and 4. To enhance the reliability of V&V, a larger number of benchmarks were used in this study (28 samples, discharged from Novovoronezh-4 and 182 FAs discharged from X2).

Isotope inventory prediction plays a crucial role in back-end cycle analyses. As various VVERs approach the end of their license periods,

* Corresponding author. Department of Nuclear Engineering, Ulsan National Institute of Science and Technology, 50 UNIST-gil, Eonyang-eup, Ulju-gun, Ulsan, 44919, Republic of Korea.
E-mail address: deokjung@unist.ac.kr (D. Lee).

https://doi.org/10.1016/j.net.2023.12.032
Received 13 September 2023; Received in revised form 19 November 2023; Accepted 12 December 2023
Available online 22 December 2023

the demand for VVER SNF analyses increases. Specifically, 12 VVERs (including Novovoronezh NPP4) reached the end of their license period (*i.e.*, shutdown) by around 2020 [4]. Novovoronezh Unit 4 has been operational since March 24, 1973 [9] and is projected to close by 2033 (*i.e.*, 2018 plus an extended license period of 15 years) [10]. To address this demand, various code systems have been developed and employed for SNF analysis: WIMS/ABBN, CASMO4, MONK7B, MCNP4B, HELIOS1.4, TWODANT, SCALE, and ORIGEN [11,12]. To improve the competitiveness of the in-house nodal diffusion code, RAST-V, a VVER SNF analysis calculation module was developed and implemented.

The suggested calculation scheme has two main features: (1) the analysis is performed without requiring an additional code system for SNF analysis after the 3D core simulation, as the nodal code RAST-V directly predicts the isotope inventory and calculates the source term based on it, reflecting the 3D core simulation time; and (2) Lagrange interpolation is used to predict the isotope inventory, replacing the need to solve the micro-depletion chain. Owing to these features, the proposed approach provides benefits in terms of the simulation time. A comparison of the simulation times was also included in this study, using the X2 reactor and STREAM SNF for the calculation [13].

Furthermore, SNF analysis was used for the following four back-end cycle analyses: (1) optimization of loading patterns in the cask model; (2) adjustment of isotope composition, which can be used in recycling (*i.e.*, pyro processing); (3) calculation of the source term; and (4) generation of a criterion during the design process of the cask and spent fuel pool. The criterion for design of cask and spent fuel pool is the upper safety limit (USL), and the burnup credit method has recently been suggested to increase the economic benefits in the field of safety analysis [14]. Burnup credit calculations were performed in this study.

With an increase in the volume of SNFs, the demand for denser racks has also increased to maximize the economic benefits within a confined space in SNF pools. The number of SNF assemblies in a given space can be increased using two primary strategies. One approach is to develop a more powerful neutron absorber for the spent fuel pool and dry cask, and the other is to provide less conservative criteria by considering isotope depletion during the design process of the cask and spent fuel pool. In the second approach, the burnup credit method was used to provide less conservative criteria for safety analysis using SNFs instead of fresh fuels for criterion generation. This approach maximizes economic benefits within the USL [14,15]. Safety analysis criteria were established by considering the bias and bias uncertainty of the geometric and material modeling parameters, isotope composition, and calculation code. The bias and bias uncertainties of the isotope compositions were calculated to establish the USL. The VVER-440 cask model [12] was used in this study.

In the updated SNF analysis module, the HDF5 [16] format is now employed to generate a number density (ND) file, aiming to reduce computation time, particularly during preprocessing. The HDF5, a hierarchical data format developed by the HDF Group, efficiently stores data with indices, facilitating easier data retrieval compared to traditional text files. This enhancement in the SNF module leads to notable reductions in both simulation time and memory usage. In details, HDF5 achieves significant file compression, reducing file sizes to 50 % of their original size. In addition, pin-wise calculations using HDF5 files are completed within 1 s, markedly faster than the 60 s required by calculation modules in previous studies [1].

The remainder of this paper is organized as follows: In Section 2, the calculation features for the SNF analysis are detailed. The V&V results with Novovoronezh-4 FAs, using 28 pin samples for the calculation, are presented in Section 3. Code-to-code comparisons were performed using CASMO-4E [17,18] with different neutronics libraries, JEF-2.2, and ENDF/B-VI.0. Furthermore, detailed comparisons were made regarding the neighboring effect of FAs in the core, uncertainty owing to neutronics data, and uncertainty owing to the standard deviation of the burnup indicator. In Section 4, the application of SNF analysis with the X2 reactor are presented, and the simulation time with that of STREAM to highlight the benefits of RAST-V is compared. The burnup credit calculation as an application of the developed code system using the Novovoronezh-4 samples is presented in Section 5.

2. Code system

2.1. STREAM/RAST-V two-step method

The STREAM/RAST-V, a two-step code system consisting of lattice code (STREAM) and nodal diffusion code (RAST-V), was used in the calculations for the VVER reactors. Developed by UNIST, these in-house codes offer a two-step approach to 3D core simulations. The VVER analysis solver was previously successfully implemented in RAST-V and validated using VVER-440 and Kalinin-3 reactors [19,20].

The STREAM/RAST-V two-step method, validated by several benchmark problems, including Rostov-II and X2, can assess a newly developed hexagonal analysis module [8,21]. The X2 benchmark was used to evaluate multicycle calculations with depletion, rod worth, and thermal-hydraulic (TH) feedback, whereas the AER-DYN-001 and AER-DYN-002 benchmarks helped verify the transient calculation module. The SNF analysis module was updated for back-end cycle analysis of the VVER.

The newly developed VVER analysis module incorporates an advanced semi-analytic nodal method (A-SANM) [22] in the radial direction and an NEM in the axial direction [8,23]. The coarse mesh finite difference (CMFD) method was also adapted to the RAST-V for acceleration [22]. This study focuses on verifying and validating the SNF calculation module. As in a previous study involving square-type FAs [1], this method showed a substantial reduction in simulation time compared with the one-step method, specifically, the STREAM calculation.

The calculation process used STREAM-SNF involves four steps: (1) generating few-group constants for the 3D core simulation, (2) executing the 3D core simulation with RAST-V, (3) performing re-depletion calculations for isotope composition prediction based on the operating condition history to mirror the 3D core simulation conditions using micro depletion solver implemented in STREAM, and (4) calculating the decay heat with the predicted isotope composition. Micro depletion solver implemented in STREAM employs the Chebyshev rational approximation method (CRAM) for isotope composition calculations [24].

RAST-V excels in simulations by eliminating the third step in the STREAM SNF analysis approach instead of using Lagrange interpolation for isotope composition prediction. A comparison of the simulation times, as demonstrated using the X2 benchmark, is presented in Section 4. However, 36 isotopes that exhibit significant sensitivity in calculations employ a micro-depletion chain [1,2].

Fig. 1 illustrates the calculation flow of the two-step method for the SNF analysis. STREAM provides number density (ND) files for Lagrange interpolation, and a pin-based slowing down method was employed for the resonance treatment [24]. An ND file is generated using a historical branch calculation similar to the branch calculation employed to generate a few-group constant data file. Table 1 presents the ten

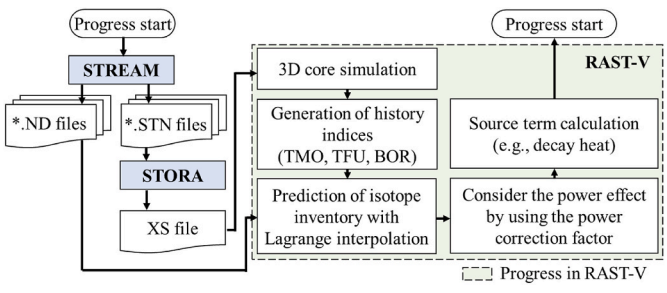

Fig. 1. Sequence of operations in VVER SNF analysis.

Table 1
Operating conditions for history branch calculation.

#[a]	TMO[b]	TFU[c]	BOR[d]	#	TMO	TFU	BOR
1[e]	TMO_1	TFU_1	BOR_1	6	TMO_1	TMO_1 – 20 K	BOR_1
2	TMO_1 – 40 K	TFU_1	BOR_1	7	TMO_1	1500 K	BOR_1
3	TMO_1 – 20 K	TFU_1	BOR_1	8	TMO_1	TFU_1	0.1 ppm
4	TMO_1 + 20 K	TFU_1	BOR_1	9	TMO_1	TFU_1	BOR_1 * 2
5	TMO_1 + 40 K	TFU_1	BOR_1	10	TMO_1	TFU_1	2400 ppm

a is the number index of history branch calculation; *b* is moderator temperature condition; *c* is fuel temperature; *d* is the boron concentration; *e* is reference; reference condition is defined as (TMO_1, TFU_1, BOR_1).

conditions used in the historical branch calculation. The history branch calculation involves three primary parameters for isotope prediction using Lagrange interpolation: moderator temperature in the range of TMO_1 – 40 K to TMO_1 + 40 K, fuel temperature from TMO_1 – 20 K to 1500 K, and boron concentration from 0.1 ppm to 2400 ppm. Here, TMO_1 represents the moderator temperature established in the reference branch. In this calculation approach, TMO_1 – 20 K is specifically considered for fuel temperature to generate the few-group constants and number density files essential for predicting isotope inventory. This calculation condition is deliberately chosen to simulate the hot zero power condition, where TMO_1 – 20 K is applied to both moderator and fuel temperatures.

The differences between historical branch and branch calculations are depicted in Fig. 2. The base calculation is a depletion calculation under reference conditions (C1 condition in this figure), whereas the branch calculation is performed at a specific burnup step with the following altered parameters (C2): boron concentration, fuel temperature, moderator temperature, and control rod position. The historical branch calculation is a depletion calculation with changing parameters before the depletion calculation (C3). The time-step intervals for the calculations were identical to those of the base calculation.

The ND and cross-section (XS) data files contained the ND of the isotopes and few-group constants used in the 3D core simulation, respectively. STORA, the linking code, reformats the few-group constants for RAST-V.

2.2. Isotope inventory prediction module

For the isotope inventory prediction, Lagrange interpolation [25] was used based on the ND file generated using STREAM. Three main conditions, moderator temperature, fuel temperature, and boron concentration, were factored into the interpolation to reflect the 3D core simulation conditions. The calculation assumes that each operating condition individually influences the ND. The generation of isotope inventories is based on the summation of the ND differences. The total calculated ND includes the sum of the effects caused by varying the calculation conditions, as shown in Equation (1).

$$\begin{aligned} ND_{total} &= ND_{base} + \Delta ND_{BOR} + \Delta ND_{TFU} + \Delta ND_{TMO} = ND_{base} + ND_{BOR} \\ &\quad - ND_{base} + ND_{TFU} - ND_{base} + ND_{TMO} - ND_{base} = ND_1 \\ &\quad + \sum_{i=1}^{5}\left(\prod_{j=1,j\neq i}^{5}\frac{h-TMO_j}{TMO_i-TMO_j}\right)ND_i - ND_1 \\ &\quad + \sum_{i=1,(i<2\ or\ i>5)}^{7}\left(\prod_{j=1,j\neq i,(i<2\ or\ i>5)}^{7}\frac{h-TFU_j}{TFU_i-TFU_j}\right)ND_i - ND_1 \\ &\quad + \sum_{i=1,(i<2\ or\ i>7)}^{10}\left(\prod_{j=1,j\neq i,(i<2\ or\ i>7)}^{10}\frac{h-BOR_j}{BOR_i-BOR_j}\right)ND_i - ND_1 \end{aligned} \tag{1}$$

where ND_{total} is the total ND used for the isotope prediction. The notation of ND represents the number density; ND_{base} is the base ND generated by the reference condition; ΔND_{TFU}, ΔND_{TMO}, and ΔND_{BOR} are the ND difference due to the fuel temperature, moderator temperature, and boron concentration between reference condition and history index (*i.e.*, accumulated 3D core conditions including TMO, TFU, and BOR), respectively, where TFU is the fuel temperature, TMO is the moderator temperature, and BOR is the boron concentration. The TMO, TFU, and BOR use the 4th, 2nd, and 3rd order Lagrange interpolations, respectively [1,2]. To reflect the 3D core conditions during the simulation, history indices were used. A history index is defined by Equation (2) [1,2]. This value was recognized as the cumulative variable of the 3D core conditions during the simulation. This paper uses three conditions: TMO, TFU, and BOR.

$$\boldsymbol{h} = \frac{\sum_{i=1}^{n} x_i \Delta t_i}{\sum_{i=1}^{n} \Delta t_i} \tag{2}$$

where x represents the parameters TMO, TFU, and BOR, where Δt, i, and n are the time interval, index of the burnup step, and index of the total number of time steps, all used in the 3D core simulation, respectively. A power correction factor (PCF) was used to adjust for different power levels, as shown in Equation (3).

$$ND_{correct} = ND_{total} * PCF \tag{3}$$

where $ND_{correct}$ is the ND adjusted by the PCF and ND_{total} is the calculated ND obtained from Equation (1). The detailed formula of the PCF is described by Ref. [22]. The PCF is derived using Bateman equation [22, 26]. Bateman equation is presented in Equation (4).

$$N_i(t) = \frac{1}{g_i}\sum_{k=1}^{i}\left\{N_k(0)\left(\sum_{j=k}^{i} c_{jk}^{i} e^{-l_i t}\right) + y_k\left(\beta_k^i - \sum_{j=k}^{i}\frac{c_{jk}^{i}}{l_j}e^{-l_j t}\right)\right\} \tag{4}$$

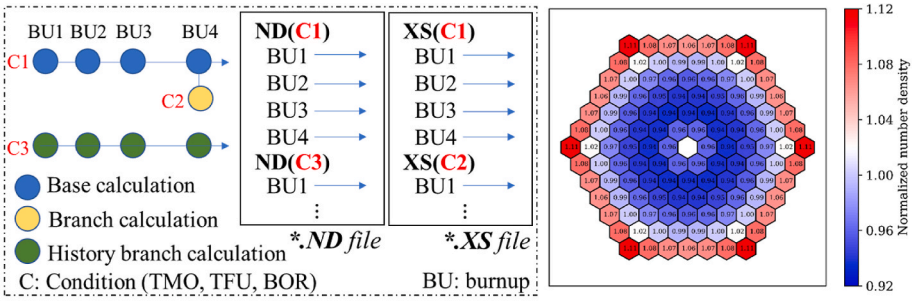

(a) Generation of number density file and cross section file (b) Distribution of number density

Fig. 2. Generation of ND and XS files.

where the $c_{jk}^{i} = \frac{\prod_{l=k}^{i} g_l}{\prod_{l=k,l\neq j}^{i} (l_l - l_j)}$, and $\beta_k^i = \frac{\prod_{l=k}^{i} g_l}{\prod_{l=k}^{i} l_l}$. By using the follows relationships, Equation (4) could be simplified as Equation (5): $g_1 \simeq \lambda_1$, $l_1 \simeq \lambda_1$, $c_{11}^1 \simeq \lambda_1$, and $\beta_1^1 = \frac{g_1}{l_1} \simeq 1$.

$$N_1(t) = N_1(0)\exp(-\lambda_1 t) + \frac{1}{\lambda_1} y_1 (1 - \exp(-\lambda_1 t)) \quad (5)$$

About this case, precursor effect is only considered. Second term of Equation (5), $\frac{1}{\lambda_1} y_1 (1 - exp(-\lambda_1 t))$, has been refined as $\mu_j F(1 - exp(-\lambda_1 t))$ consulted from the previous studies [27,28], where μ_j is the coefficient and F is the ratio of power difference between power used in history branch calculation and power calculated by 3D core simulation at specific point. Power correction factor has been generated based on this relationship.

Fig. 1 illustrates the workflow of the VVER SNF analysis. The process involves three main codes: STREAM, STORA, and RAST-V. As depicted, conditions from 3D core simulations are used for computation. The STREAM code generates few-group constants, which are collected in a file, and produces ND data in an ND file. STORA, serving as the linking code, reformats these few-group constants and creates a XS data file. RAST-V, a nodal diffusion code, is employed to conduct 3D core simulations, generating conditions that are compiled as a 3D core simulation history. These histories, encompassing fuel temperature, boron concentration, and moderator temperature, are then used for Lagrange interpolation. PCF is generated using the Bateman equation and applied in the calculation. Finally, source-term calculations are performed using the predicted isotope inventories.

Fig. 3 shows the PCF. Fig. 3 (b) and Fig. 3 (c) present the power histories for each assembly. For calculations, assembly-wise power is employed. In the case of FA-wise calculations, the corresponding FA-wise power data is utilized. $ND_{STREAM,\ P1}$ and $ND_{STREAM/RAST\text{-}V,\ P1}$ were the outputs computed based on Fig. 3 (b), whereas $ND_{STREAM,\ P2-P4}$ and $ND_{STREAM/RAST\text{-}V,\ P2-P4}$ were the outputs calculated based on Fig. 3 (c). The power conditions oscillated in a $4 \rightarrow 2 \rightarrow 4 \rightarrow 2 \rightarrow 4$ pattern. This figure also includes a PCF. The reference is defined as $ND_{STREAM,\ P2-P4}$ divided by $ND_{STREAM,\ P1}$, and the 'without PCF' case is defined as $ND_{STREAM/RAST\text{-}V,\ P1}$ divided by $ND_{STREAM,\ P1}$. The 'with PCF' case is defined as $PCF*ND_{STREAM/RAST\text{-}V,\ P2-P4}$ divided by $ND_{STREAM,\ P1}$. As shown in Fig. 3 (a), the 'with PCF' case aligned well with the reference. ND_{3D} is the ND generated by the 3D core simulation, whereas reference uses the STREAM calculation with the power scenario in Fig. 3 (c). ND_{2D} is the ND generated by the 2D calculation used to generate the ND file; specifically, the power used in the STREAM calculation. P4 and P2 are the relative power conditions used in Fig. 3. The values of P2/P1, P4/P1, and P4/P2 were 2, 4, and 2, respectively. The beta decay effect of ^{141}La was considered during generation of the PCF. In these calculations, ^{141}La served as the precursor for the ^{141}Ce isotope.

Throughout the calculation process, a pin-wise calculation was performed with a pin-wise ND distribution and this data file is used for Lagrange interpolation instead of FA-wise ND file illustrated in Fig. 1. Sample pin-wise ND distribution is illustrated in Fig. 2 (b). A FA-wise ND file was generated using the micro-depletion chain presented in the nodal diffusion code RAST-V.

3. Validation novovoronezh NPP unit 4

Validation was performed using 28 VVER-440 samples discharged from the Novovoronezh NPP Unit 4 [6]. Since 1970s, reactors have been planned for decommissioning by the 2030s [10]. This benchmark problem was formulated for back-end cycle analyses, such as cask design and criticality analysis with burnup credit [6]. The Novovoronezh NPP Unit 4 benchmark was developed under the #2670 ISTC project [29], and the V&V of RAST-V were performed. Additionally, since STREAM newly incorporated the hexagonal FA analysis module into the code, STREAM V&V was also performed. To validate the calculation capabilities of STREAM, a code-to-code comparison was conducted using CASMO-4E with different neutronic libraries, and the code results were derived from previous studies [17,18]. Table 2 outlines the specifications of the Novovoronezh-4.

The FA specifications are presented in Table 2 [29], with an enrichment of fresh UO_2 fuel of 3.6 wt %. Fig. 4 illustrates the radial layout and axial configuration of the FAs. Fig. 4 (a) and Fig. 4 (b) show

Table 2
Specification of novovoronezh NPP 4 FA

Parameter	Value	Unit	Parameter	Value	Unit
Reactor type	VVER-440		Shroud inner pitch	14.02	cm
FA pitch	14.7	cm	Shroud thickness	0.40	cm
No. of fuel rods	126	–	^{235}U enrichment	3.6	wt.%
No. of guide tube	1	–	Pin pitch	1.22	cm
No. of cycles	4 (15^{th}–18^{th} cycle)	–	Pellet diameter	0.37825	cm
Fabrication data	1987	–	UO_2 fuel density	10.6	g/cm^3

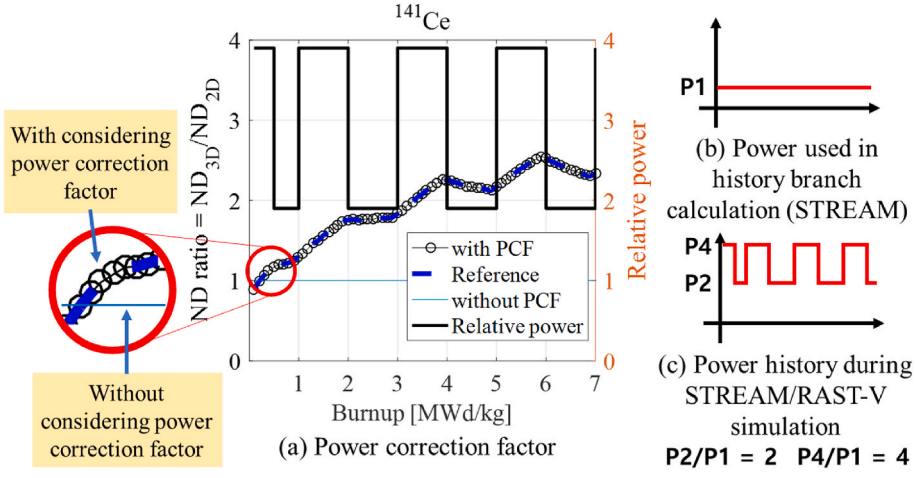

Fig. 3. Effects of PCF on isotope prediction.

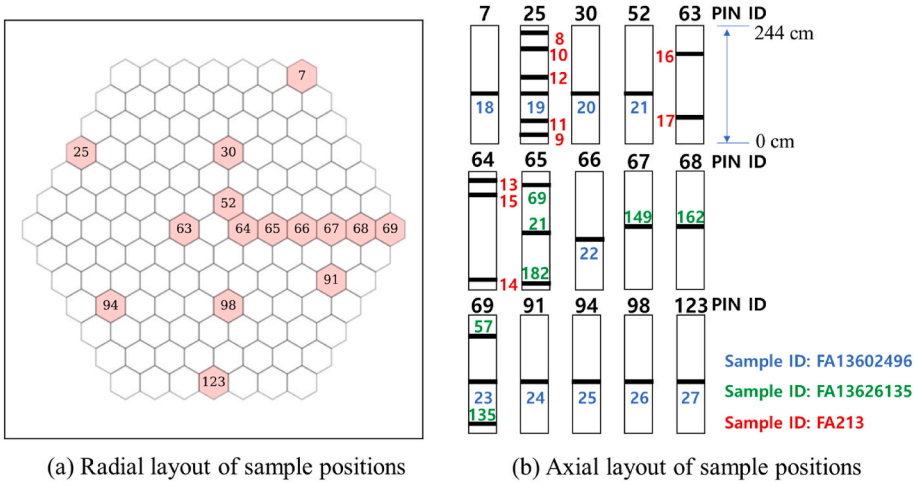

(a) Radial layout of sample positions (b) Axial layout of sample positions

Fig. 4. Radial and axial layout of Novovoronezh NPP 4 FA

the sample pin locations in the radial layout of the FA and the axial locations of the pin samples, respectively. A two-step method was applied to the calculations, considering the overhaul period. A total of 28 pin samples, discharged from three fuel assemblies: 13602496, 213, and 13626135, were used. FA ID 13602496 has the burnup range of 37.2–44 MWd/kg and axial height of 87.5 cm. FA ID 213 has the burnup range of 20.4–38.7 MWd/kg and axial height of 12.5–228.5 cm. FA ID 13626135 has the burnup range 22.86–46.3 MWd/kg and axial height of 10–215 cm. The overhaul periods were set to 67, 32, and 70 d for the intervals between cycles 15 and 16, 16 and 17, and 17 and 18, respectively. The calculation conditions were established based on reference [30].

STREAM generates two-group constants using method of characteristics (MOC) with a ray spacing of 0.05 cm; the numbers of azimuthal and polar angles was 48 and 6, respectively. The ENDF/B-VII.0 [31] library was used for the calculations.

Comparison results are depicted in Figs. 5–13, which show the relative differences, with one standard deviation (1σ) of the measurement. The measurement results were obtained from the literature [6,29,30]. However, ^{246}Cm of sample ID 57 was not provided by the benchmark [6]; therefore, the relative differences are not included in Fig. 6.

The CASMO-4E results, calculated using the ENDF/B-VI.0 and JEF-2.2 libraries, were sourced from Ref. [18]. RAST-V employs the ENDF/B-VII.0 library for calculations. Most isotopes were within ±10 % of the difference boundaries.

The ^{245}Cm and ^{246}Cm isotopes exhibited the largest differences compared to the measurements as shown in Figs. 7–11. These isotopes are secondary fission products [14,15], and their absolute quantities are much smaller than those of actinides and the main fission products. Consequently, the relative difference could be large compared with the other isotopes. Moreover, as shown in a previous study [2], Cm isotopes exhibit high sensitivity to burnup conditions; a burnup difference of 1 % results in up to an 8 % difference in the Cm isotope quantity. In a previous study [2], ASTM E 321-79 was used to measure the burnup, and this method had a standard deviation of up to 3 % in the measured burnup. Since this study employed an average burnup of three measurements [6], burnup uncertainty could have affected the large differences in the Cm isotopes. Furthermore, as previously indicated [32], ^{245}Cm and ^{246}Cm have large uncertainties owing to the cross-sectional library and input parameters. A prior uncertainty study using the STREAM/RAST-V code system revealed that isotope composition uncertainties could reach 31.10 % (maximum uncertainty is occurred at ^{246}Cm of U1 with ENDF/B-VII.1 covariance library) [32]. Although these results have limitations and cannot be directly reflected in this calculation, this uncertainty signifies that the Cm isotope difference can be attributed to uncertainties in the cross-sectional data and design/-operating parameters [33]. Furthermore, the Cm measurement method is mass spectrometry [6,34,35]; thus, this measurement-method

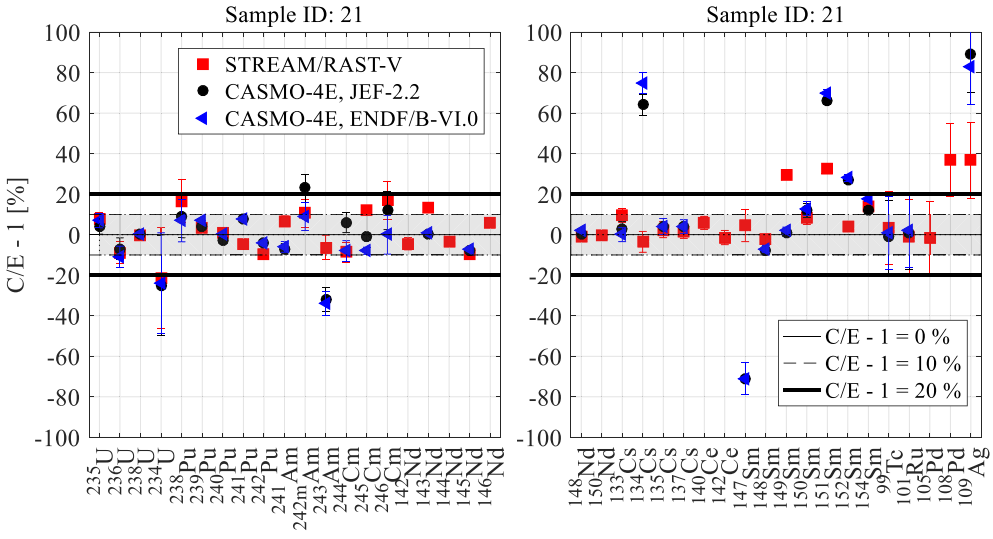

Fig. 5. Isotope composition difference of sample ID 21 from FA ID 1326135.

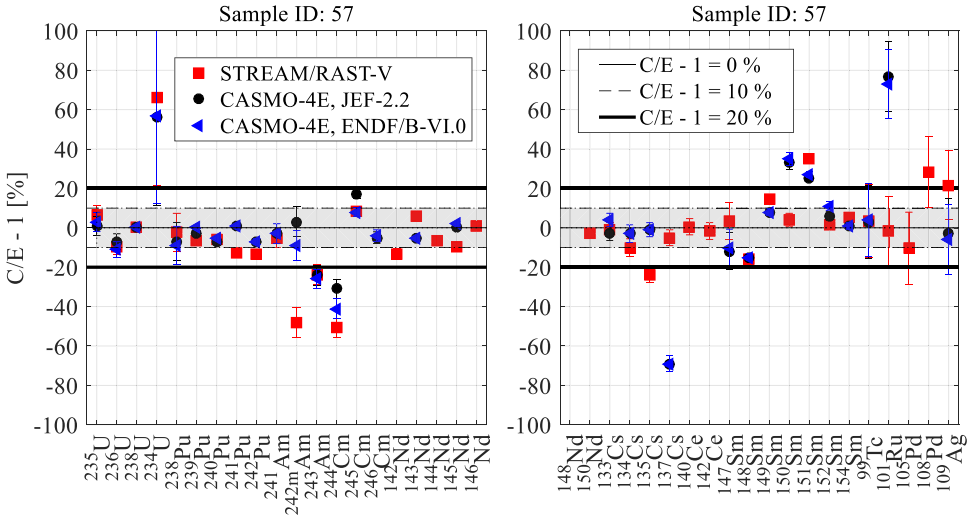

Fig. 6. Isotope composition difference of sample ID 57 from FA ID 1326135.

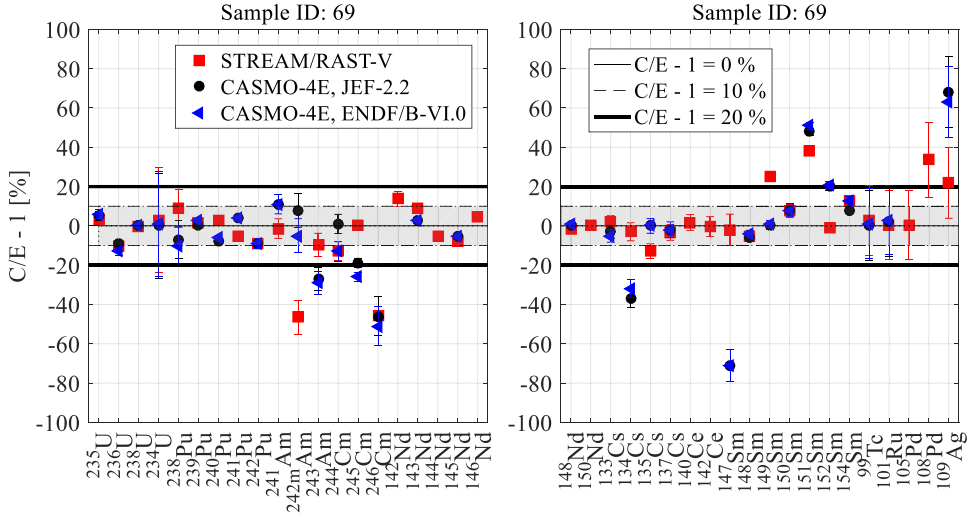

Fig. 7. Isotope composition difference of sample ID 69 from FA ID 1326135.

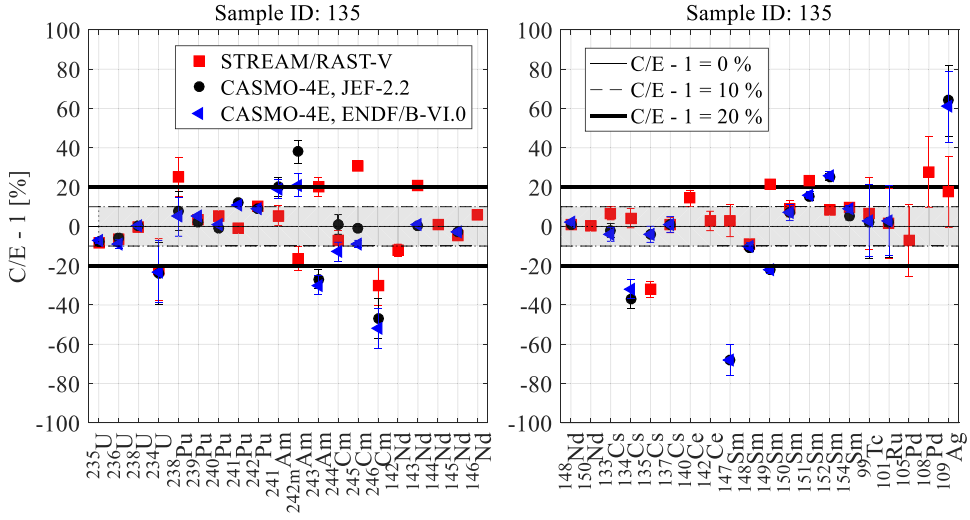

Fig. 8. Isotope composition difference of sample ID 135 from FA ID 1326135.

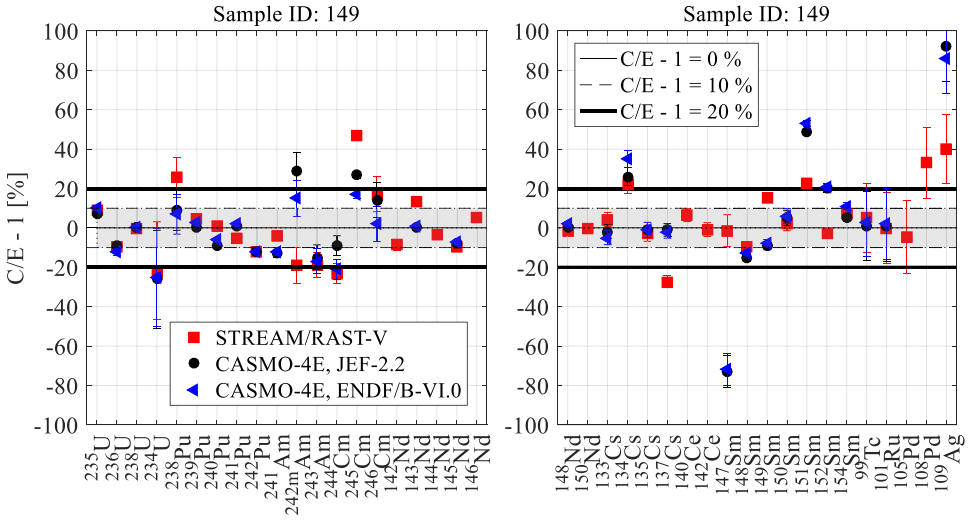

Fig. 9. Isotope composition difference of sample ID 149 from FA ID 1326135.

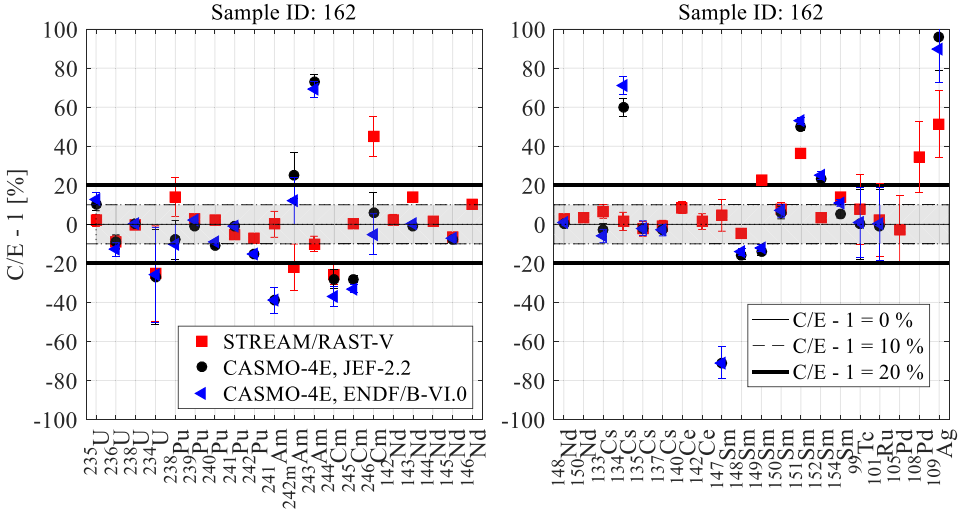

Fig. 10. Isotope composition difference of sample ID 162 from FA ID 1326135.

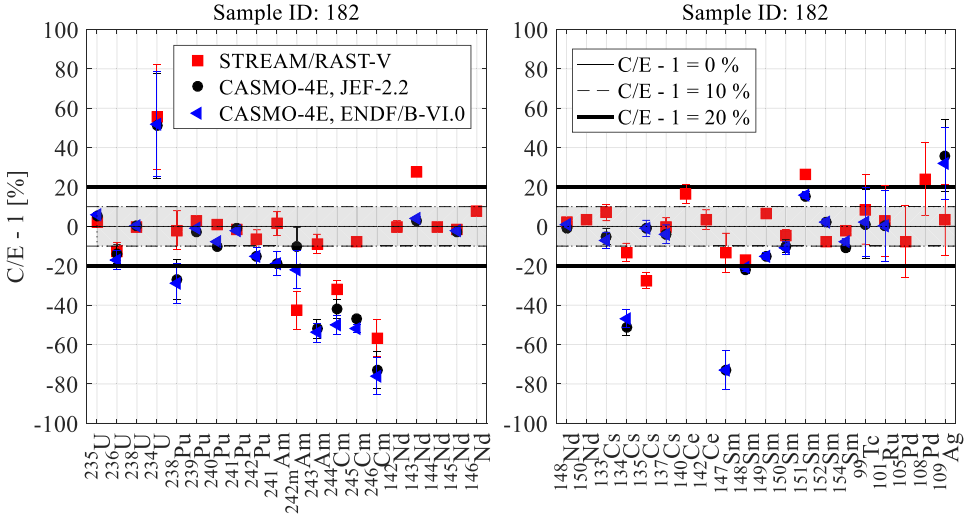

Fig. 11. Isotope composition difference of sample ID 182 from FA ID 1326135.

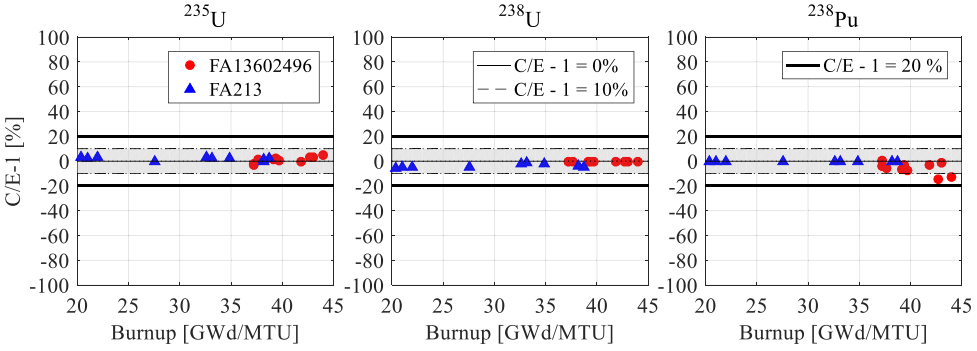

Fig. 12. Relative differences of ^{235}U, ^{238}U, and ^{238}Pu from FA ID 13602496 and FA ID 213.

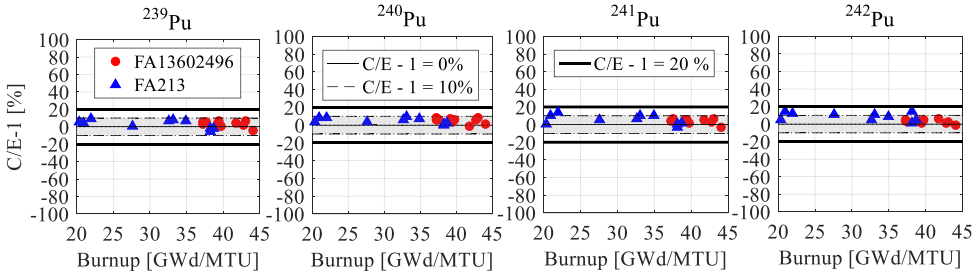

Fig. 13. Relative differences of ^{239}Pu, ^{240}Pu, ^{241}Pu, and ^{242}Pu from FA ID 13602496 and FA ID 213.

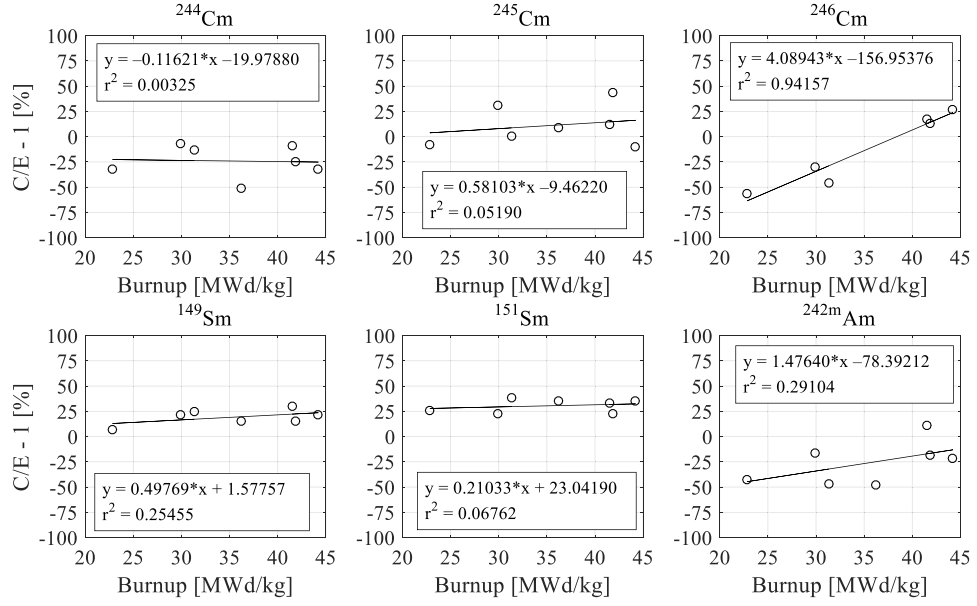

Fig. 14. Linear tends with isotopes which have large difference compared with experimental data (burnup).

uncertainty could contribute to the Cm differences.

To understand the reasons for these large differences, various sensitivity analyses were conducted, as detailed in Sections 3.1 to 3.3. These sections are associated with the effects of neighboring FAs in the core, uncertainty due to neutronic data, and uncertainty due to the standard deviation of the burnup indicator, respectively. Prior to comparing these effects, a trend analysis was performed with the burnup and axial height to identify the main causes of these large differences (Figs. 14 and 15). In statistical analysis, the notation of r^2 is used to signify the goodness of fit [36]. A value of this coefficient closer to 1 indicates a better fit to the linear trend [2]. As demonstrated in Fig. 14, isotopes ^{246}Cm, ^{149}Sm, and ^{242m}Am showed significant correlations with burnup, more so than other isotopes. Furthermore, as depicted in Fig. 15, ^{151}Sm demonstrated a strong correlation with axial position. This indicates that ^{151}Sm was significantly influenced by the neighboring isotopes. This analysis was performed since samples 182 and 135 showed large differences compared to the other samples. This trend may reflect the effect of the leakage near the edge of the FA in the axial direction. The results in Figs. 5–11 were used to investigate the sensitivity.

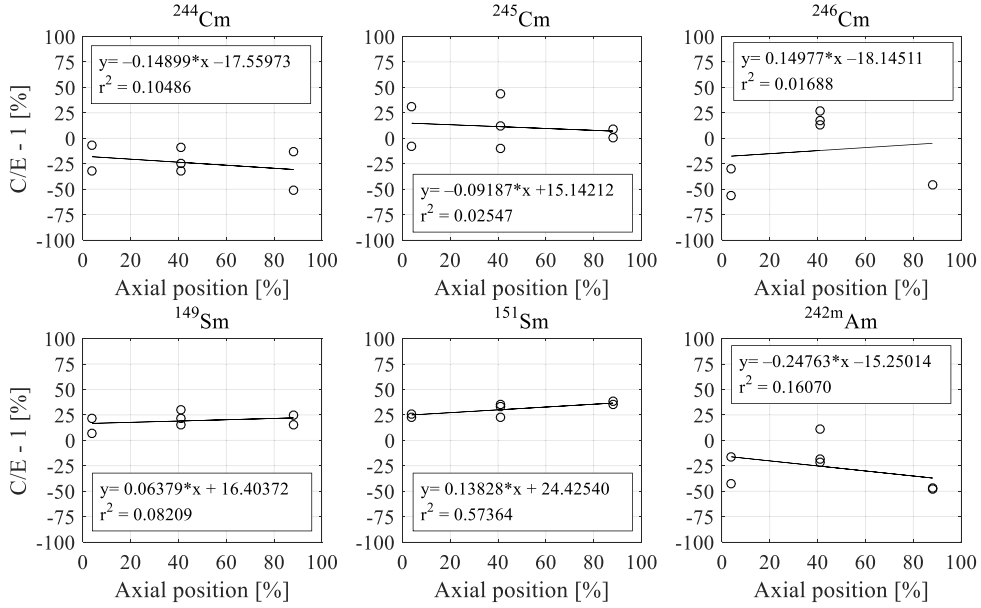

Fig. 15. Linear tends with isotopes which have large difference compared with experimental data (axial position [%]).

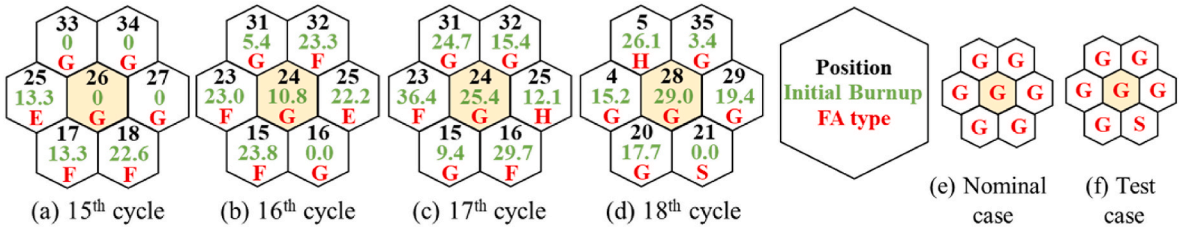

Fig. 16. FA position in core.

3.1. Neighboring effect

In this section, the impact of neighboring effects on SNF analysis using the Novovoronezh-4 FA model is presented. Noteworthily, during SNF analysis, neighboring FAs are typically not considered, implying the calculations to be based on a single FA model. However, these measurements stem from a core model that naturally encompasses the effects of neighboring FAs.

As outlined in the specification document [6], FA 13626135 is surrounded by other FAs, as shown in Fig. 16, where the yellow FA represents the calculated FA position. As shown in the figure, different types of FAs with variable initial burnups surround the calculated FA. This could significantly affect the isotope inventory of the calculated FA. The FAs of types G, H, E, and F are composed of 3.6 wt % enriched UO_2 fuel, while type S FA uses 2.4 wt% enriched UO_2 fuel.

To investigate the effects of neighboring FAs, a supercell-type calculation model was used, as illustrated in Fig. 16 (e) and Fig. 16 (f). This model was devised to consider the conditions outlined in Fig. 16 (d). Fig. 16 (e) and Fig. 16 (f) show the nominal and test cases, respectively.

The tests were conducted at a power level of 4 MW for 30 d using the supercell-type calculation models illustrated in Fig. 16. FA13626135, shown in Fig. 4, was used for comparison. The relative differences due to neighboring effects, as a part of this sensitivity study, are listed in Table 3. Especially, four pins located in FA13626135 are compared. As is evident from the table, the Cm isotopes exhibit high sensitivity to

Table 4
Uncertainty of sample ID 21.

Isotope	^{242m}Am	^{244}Cm	^{245}Cm	^{246}Cm	^{149}Sm	^{151}Sm
Uncertainty* [%]	21.70	9.04	14.21	21.35	4.64	5.82

* Uncertainty is defined as $\sigma/\mu * 100$ [%]: σ and μ are the standard deviation and average of number density calculated by perturbed 500 samples.

Table 3
Relative difference with sensitivity study of neighboring effect.

Pin ID	^{242m}Am	^{244}Cm	^{245}Cm	^{246}Cm	^{149}Sm	^{151}Sm	^{235}U	^{239}Pu
65	3.52[a]	16.49	20.33	26.11	−0.52	1.20	−4.39	0.65
67	3.07	16.25	19.95	25.77	−0.74	1.12	−4.72	0.49
68	2.59	15.99	19.52	25.37	−0.94	1.07	−5.13	0.34
69	1.89	15.56	18.89	24.72	−1.17	1.08	−5.79	0.16

a is relative difference $C_{test\ case}/C_{nominal\ case} - 1$ [%]. The notation of C is the calculated results. Layout of nominal case and test case are illustrated in Fig. 16 (e) and Fig. 16 (f), separately.

neighboring effects.

3.2. Neutronics data uncertainty

The ENDF/B-VII.1 neutronics library was used for this calculation. As indicated in previous studies [33,37], the ENDF/B-VII.1 neutronics library carries inherent uncertainty, which can affect the calculation results [32]. The uncertainties, calculated using the ENDF/B-VII.1 covariance matrix, are listed in Table 4. The calculation used 500 perturbed cross-sectional data points. Singular value decomposition was applied to perturbed cross-sectional data [22,33,37]. A stochastic sampling method was used for the computation. The calculation module was previously verified using SCALE 6.2.2 [22]. The isotopes ^{242m}Am, ^{245}Cm, and ^{246}Cm showed significant discrepancies, as illustrated in Table 4. In the uncertainty quantification analysis, the discharged burnup and cooling periods are kept consistent by employing a stochastic sampling method, ensuring consistent calculation conditions [6]. This suggests that the uncertainties arising from the neutronics data can cause significant differences in the quantities of ^{242m}Am, ^{245}Cm, and ^{246}Cm.

3.3. Burnup indicator

The sensitivity of the calculated results (predicted isotope inventories) to burnup, as indicated in a previous study [2], are discussed in this section. Table 5 presents the results of the sensitivity analysis using the burnup indicator. ^{148}Nd displays a standard deviation of approximately 1 % according to Ref. [30]. The impact of the standard deviation of the burnup indicator on the variance in the isotope prediction is discussed in this section. When the burnup indicator (^{148}Nd) changed by 1 %, the isotopes changed by up to 11 %. As shown in the table, ^{245}Cm, ^{246}Cm, and ^{242m}Am exhibited significant differences. This trend aligns with the linear trend analysis shown in Fig. 14, suggesting that the standard deviation of the burnup indicator could influence the results of the isotope prediction.

4. Application of SNF analysis with X2 reactor model

In this section, the evaluation of the computational performance of RAST-V in a 3D core simulation through a verification study performed using the X2 reactor is presented. Calculations for Cycles 1 and 2 were conducted. The STREAM code was utilized for code-to-code comparison, as it directly solves micro depletion, unlike the Lagrange interpolation used in the RAST-V SNF analysis approach. STREAM SNF has been previously validated [13,38].

The X2 reactor is a model VVER-1000 reactor with a thermal power of 3,000 MW [7,39]. Table 6 provides the detailed specifications for the X2 reactor [7,39]. The reactor is loaded with 163 FAs. The active height is 355 cm, and 20 axial calculation nodes were used in this active height region. Two reflector models, each designed for a height of 30 cm, were used in this calculation. Three different FA types were used for comparison. The 390GO and 30AV5 FAs contained a gadolinia fuel pin, and the 22AU FA consisted solely of UO_2 fuel pins. This benchmark model has been previously verified [8]. CBC calculation results are summarized in Table 7.

Table 5
Sensitivity study with burnup indicator.

Sample ID Isotope	21	149	162	57	135	182	69
^{242m}Am	−6.93	−2.37	−1.11	0.40	10.73	−0.70	−0.29
^{244}Cm	−2.87	1.99	2.71	2.41	4.80	3.24	6.36
^{245}Cm	−11.12	4.32	4.20	6.52	7.70	6.10	9.82
^{246}Cm	−11.22	2.80	7.61	-[a]	5.41	3.67	8.34
^{149}Sm	−2.72	2.48	0.31	0.26	0.19	0.24	−3.00
^{151}Sm	−3.89	−0.47	0.28	0.42	0.38	0.24	0.56

a lack of measurement in benchmark specification [6].

Table 6
Specification of X2 reactor.

Parameter	Value		Unit
Number of fuel assemblies	163		–
Number of axial calculation nodes	21 (FA region) + 4 (reflector region)		–
Thickness of reflector (Top/Bottom)	30		cm
Active height	355		cm
Number of UO_2 fuel pins and enrichment	22AU	312/2.2	#/wt.
	390GO	240/4.0, 66/3.6	%
	30AV5	303/3.0	
Number of gadolinia pins (wt.% Gd_2O_3/^{235}U)	22AU	–	–
	390GO	6 (5.0/3.3)	
	30AV5	9 (5.0/2.4)	
FA pitch	23.6		cm
Fuel pin pitch	1.275		cm
Flow rate	88,000		m^3/h

Table 7
Root mean square (RMS) difference of CBC [g/kg].

Cycle	1	2
STREAM/RAST-V	0.13 (=40 ppm[a])	0.12 (=18 ppm)
BIPR7A [39]	0.29 (=51 ppm)	0.47 (=82 ppm)
CASMO-4/DYN3D [39]	0.54 (=94 ppm)	0.40 (=70 ppm)

a is converted as the ppm by using the 1 g/kg = 174.88 ppm [7].

Fig. 17 shows the loading and sample patterns of X2 reactor. A two-step method was used for the calculation, and Lagrange interpolation was performed based on ND files generated by STREAM with MOC rays of 0.03 cm, 96 azimuthal angles, and 6 polar angles. STREAM was used for code-to-code comparison, as it directly solves the Bateman equation to predict the isotope inventory. The detailed calculation scheme is described in Section 2.

A total of 91 samples were used for comparison, and the sample positions are presented in Fig. 17 (c) and Fig. 17 (d). Fig. 17 (c) displays the FAs with indices. Fig. 17 (d) shows the locations of the samples compared with the shuffling positions (*i.e.*, the positions of the FA in cycle 1). All the colored FAs in Fig. 17 (a) are used in Fig. 17 (b). The selected samples in Fig. 17 (b) are twice-burned FAs. Colored FAs located in Fig. 17 (a) and Fig. 17 (b) were used for comparison. Fig. 18 shows the comparison results with average relative differences and standard deviations. STREAM applies a reflective boundary and uses the node-wise operation history of the 3D core simulation, including the fuel and moderator temperatures and boron concentration conditions. A total of 47 isotopes were analyzed. The isotopes of ^{90}Sr, ^{137}Cs, ^{90}Y, and ^{137m}Ba, which contribute significantly to the decay heat (~30 % contribution) [1], were selected for comparison with a previous study [1]. These isotopes aligned well with STREAM (*i.e.*, the direct micro-depletion solver solution). As the figure displays, all isotopes were within the ±20 % error boundary, and most isotopes exhibited a difference within ±10 %. This pattern aligns with previously observed trends [2]. As demonstrated in the preceding section 3, secondary fission products (*e.g.*, ^{245}Cm and ^{246}Cm) show large differences compared to the actinide isotopes (*e.g.*, ^{235}U and ^{238}U) as shown in Figs. 5–11. This discrepancy could have been influenced by the absolute amount of fission products, which was substantially less than that of the actinide isotopes. In addition, as discussed in Section 3.1, the neighboring effect was shown to affect these results. The 91 samples were compared in each cycle, meaning, a total of 182 samples were used for comparison. Fig. 19 shows the simulation times for 182 samples. Common processes, such as the generation of XSs and 3D core simulations, were not included in this comparison. The generation of ND files for RAST-V SNF analysis and SNF analysis times are compared in this figure. The detailed comparisons are presented in Table 8. These comparisons were conducted using

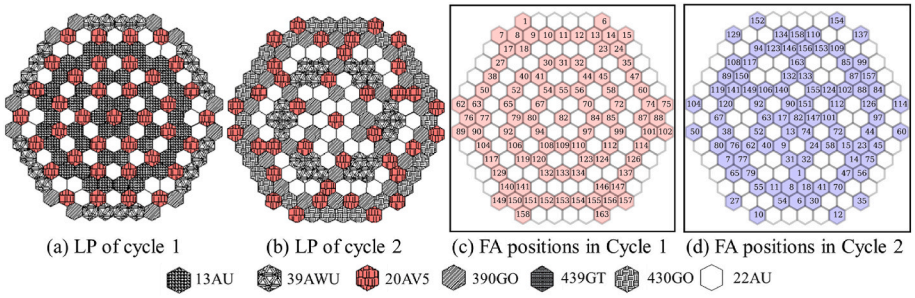

Fig. 17. Radial layout of X2 reactor and FA used in verification.

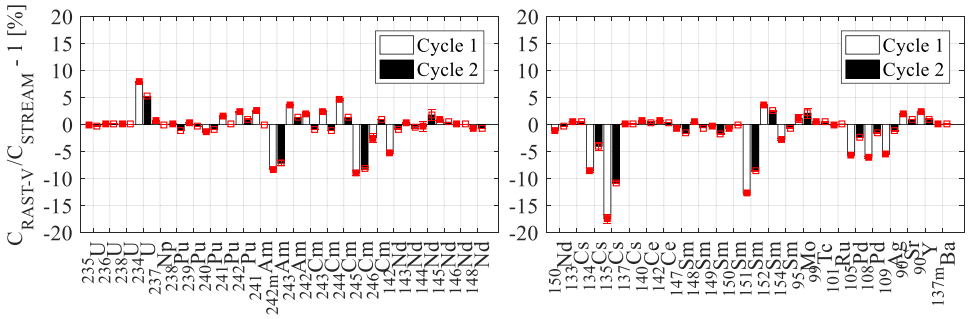

Fig. 18. Relative differences of the cycle 1 and 2 calculation.

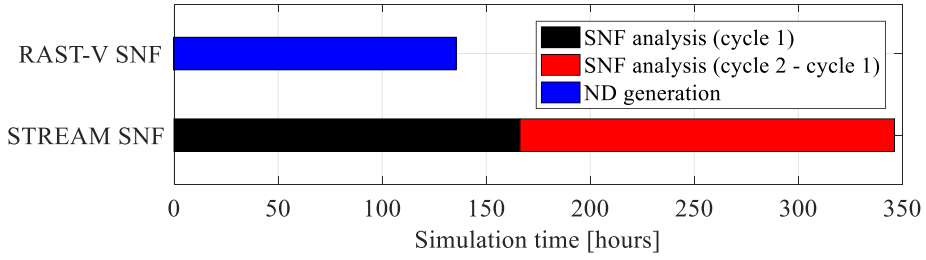

Fig. 19. Simulation time for SNF analysis.

Table 8
Detail simulation time for SNF analysis in both of analysis codes.

Parameter	STREAM SNF [hours]		RAST-V SNF [hours]
ND file generation	–		135.611[a] (20[b])
SNF analysis time	Cycle 1	166.263[a] (20[b])	0.136[a] (1[b])
	Cycle 2	345.901[a] (20[b])	

a is summation of total simulation time (*i.e.*, total simulation time of 163 FAs); *b* is the number of threads used in parallel computation. The 20 means that the 20 threads are used for calculations, and 1 is 1 thread is used for calculation.

a CPU of Intel(R) Xeon(R) CPU E5-2690 v2 @ 3.00 GHz. STREAM employs parallel OpenMP computations. The time required to generate ND files for RAST-V analysis was calculated as the sum of the simulation times for the three FAs (22AU, 390GO, and 30AV5), as the same FA type uses the same ND file. The SNF analysis time was the sum of the simulation times for the 91 samples in each cycle. As indicated in the table, RAST-V exhibits an advantage in simulation time compared with STREAM, which is 10^5 times faster, although it has a disadvantage in terms of simulation time for generating ND files. The strength of the RAST-V approach lies in the repetitive calculations, such as the SNF analysis of a commercial reactor, since a commercial reactor uses a finite number of FAs. Moreover, compared to the previous SNF analysis study of RAST-K [1], the ND file format was changed to HDF5 data format from a text file to reduce memory use and overcome speed disadvantages when reading data.

5. Burnup credit calculation with Novovoronezh-4 benchmark

In this section, the application results of the burnup credit are presented. Burnup credit was used to define the criterion for safety analysis, which is instrumental in the design process of SNF pools and dense dry casks, as previously demonstrated [40]. To maximize the economic benefits, the effect of burnup credit was considered in the criticality analysis. As burnup credit offers less conservative criteria for safety analysis, by utilizing SNFs instead of fresh FAs to establish the USL, it can contribute to economic benefits in the design process of innovative dense casks. In accordance with previous studies [14,15], major actinides and fission products were considered when establishing the criterion. The criterion for the burnup credit was set as shown in Equation (6). The k_{eff} bias and k_{eff} bias uncertainty caused by various parameters were used to establish the USL.

$$k_p + \Delta k_p + \beta_i + \Delta k_i + \beta + \Delta k_\beta + \Delta k_x + \Delta k_m \leq k_{limit} \quad (6)$$

where k_p is the calculated k_{eff} result and k_{linit} is the USL. Δk_p denotes the k_{eff} tolerance, β represents the bias, Δk_β is the criticality bias uncertainty,

and Δk_m signifies the unknown uncertainty [14]. In addition, the symbols β_i and Δk_i denote the k_{eff} bias and k_{eff} bias uncertainty associated with isotope composition, respectively [14]. Δk_x is supplemented to β. As indicated in Equation (6), the bias and bias uncertainties were calculated based on various parameters, including genetic factors, modeling parameters, computational codes, and isotope compositions. In this section, the calculation of the bias and bias uncertainty arising from the isotope composition using the isotope composition prediction module implemented in RAST-V are discussed.

The VVER-440 cask model was employed for the calculation, along with 28 Novovoronezh-4 benchmarks. The cask model obtained from the CB6 benchmark [40] was developed and published by the OCED/-NEA Working Party on Nuclear Criticality Safety (WPNCS) and the Expert Group on Burn-up Credit Criticality Safety (EGBUC) [40]. A Monte Carlo code, Serpent 2 [31], was used for the cask analysis [41], and the ENDF/B-VII.0 library served for the burnup credit calculation. STREAM generated ND files and few-group constants using a ray tracing of 0.03 cm, an azimuthal angle of 96, and polar angle of 6. The pin-based slowing-down method (PSM) [45] was employed for resonance treatment; up scattering of ^{238}U was considered; the thermal expansion effect was not included; the inflow transport approximation was used [42,43]; and the overhaul period was disregarded. A reflective boundary condition was applied to generate the few-group constants.

The application of sample burnup credit to define the safety analysis criterion are explored in this section, with the following content: Section 5.1 contains the benchmark specifications of CB6 benchmarks. This includes the verification of the VVER-440 cask in comparison with Serpent 2. This section also presents the isotope concentrations of the Novovoronezh-4 samples used in burnup calculations. Section 5.2 features the calculation results and progress of the k_{eff} bias and k_{eff} bias uncertainty associated with the isotope compositions.

5.1. Specification of benchmark problems

The VVER-440 benchmarks were utilized for the calculations, and the CB6 benchmark [12] was employed for the cask design during burnup credit computations. Fig. 20 illustrates the radial layout of the cask model. The NUREG/CR-7108 method was used to calculate the k_{eff} bias and k_{eff} bias uncertainties [14,44]. To compute the k_{eff} bias and bias uncertainty caused by isotope compositions, a total of 28 samples discharged from the Novovoronezh-4 benchmark were used. The relative difference (C/E−1 [%]) was employed to perturb the isotope composition for the calculation of k_{eff} bias and bias uncertainty, where 'C' denotes the results calculated by STREAM/RAST-V, and 'E' represents the measurement.

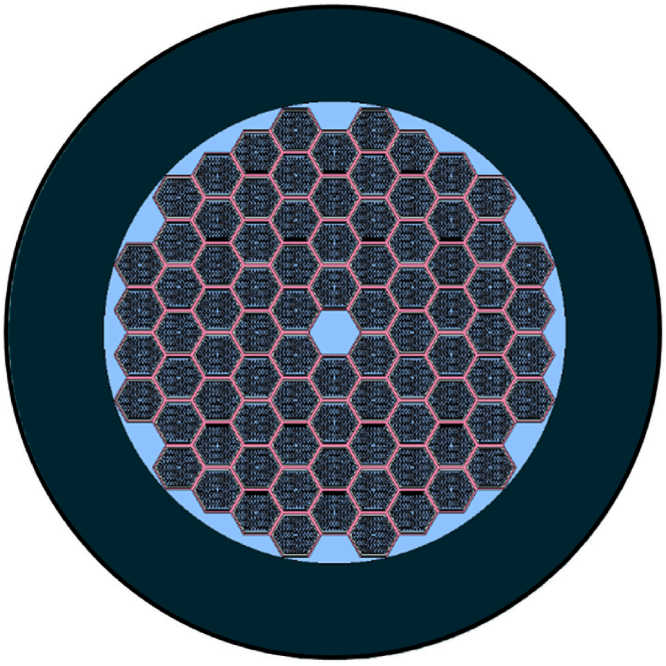

Fig. 20. Radial layout of cask model.

Table 9
Specification of cask model.

Parameter	Value		Unit
Number of FAs in cask	84		
Thickness of cask upper lid	28.8		cm
Thickness of cask lower lid	47.2		cm
Active height	244		cm
Cask height	320		cm
Inner radius of cask	90		cm
Outer radius of cask	127		cm
Material of neutron absorber plate (storage tube, intervening plate)	Storage tube	Fe (2.59[a]), Cr (0.76[b]),^{55}Mn (13.36[c]),	–
	Intervening plate	^{27}Al (231[c]), Mg (53.6[d]),^{55}Mn (13.36[c])	
Isotope composition of fresh fuel	^{235}U	9.73461E-04	#/cm^3
	^{238}U	2.16545E-02	
	^{16}O	4.52600E-02	

a, b, and *d,* are the capture cross section of ^{56}Fe, ^{52}Cr, and ^{24}Mg, separately [47]: portion of ^{56}Fe, ^{52}Cr, ^{24}Mg in Fe, Cr, and Mg are 91.754 %, 83.789 %, and 78.999 %, respectively; *c* is capture cross section of isotope, and the unit of cross section is barn [47].

Table 9 provides the specifications of the cask model [40,46]. FAs were designed with an active height of 244 cm, and 84 FAs were loaded into the cask model. Storage tubes and intervening plates that acted as neutron absorbers were used. The plates were composed of Fe, Cr, ^{55}Mn, Mg, and ^{27}Al materials. The capture XSs of these isotopes are listed in the table.

The Monte Carlo code Serpent 2 was employed for the cask computation, and the cask model was verified by comparing the results with those from previous studies to assess the calculation capability of the cask model [46]. Reference results were obtained using Serpent 2 [46]. The isotope composition of fresh fuel was used to verify the cask model; detailed information is presented in Table 9 [47]. A total of 48,000,000 neutron histories were used for the calculation, and ENDF/B-VII.0 employed for the computation. Table 10 lists the calculation results, showing differences within ±31 pcm. As indicated in the table, the differences were within 1.3 times the standard deviation boundary. The accuracy of the calculation model was comparable to that of a previous study [46], and this calculation model was used for the burnup credit analysis.

5.2. Calculation results of burnup credit

Calculation results of the benchmark problems along with the

Table 10
Verification results of cask model.

Case		Neutron history	k_{eff}	Difference[a] [pcm]
1	Serpent with ENDF/B-VII.0 [40]	105,000,000 = 50,000[a] × (2,000[b] + 100[c])	1.15355 ± 0.00007	−3 ± 25
2	Serpent with JEFF-3.1.1 [40]	105,000,000 = 50,000 × (2,000 + 100)	1.15321 ± 0.00007	31 ± 25
3	Serpent-2 with ENDF/B-VII.0	48,000,000 = 400,000 × (100 + 20)	1.15352 ± 0.00024	–

a. differences are calculated based on case3; *b* is the neutron history per cycle; *c* is the number of inactive cycles; *d* is the number of inactive cycles.

Table 11
Isotope composition for burnup credit analysis.

Isotope	Number density[a] [#/cm^3]	Number of samples	Bias ($\overline{X_i}$)	Bias uncertainty (σ_i)
^{16}O	4.52600E-02	–	–	–
^{234}U	9.59200E-08[b]	–	–	–
^{235}U	1.90000E-04	28	1.02	0.03
^{238}U	2.08100E-02	28	0.98	0.02
^{238}Pu	8.02100E-06	28	1.01	0.09
^{239}Pu	1.60000E-04	28	1.03	0.04
^{240}Pu	6.75500E-05	28	1.04	0.03
^{241}Pu	4.36300E-05	28	1.02	0.06
^{242}Pu	1.94600E-05	28	1.03	0.07
^{241}Am	1.77500E-06	–	–	–

a is based on gram density of 9.62196 g/cm^3; tf_2 is two-sided tolerance limit value and 2.673 is used for calculation [50]; *b* is the reference isotope composition provided by benchmark and this value is used for calculation as surrogate data.

burnup credit calculation incorporating isotope bias and bias uncertainty are presented in this section. In these calculations, actinides were considered to determine the k_{eff} bias and k_{eff} bias uncertainty. The burnup credit calculation was performed following the NUREG/CR-7108 document guidelines [14]. The bias ($\overline{X_i}$) and bias uncertainties (σ_i) are consolidated in Table 11. These computed values are also illustrated in Fig. 21, in alignment with the validation results for the 28 samples. Perturbed isotope compositions were employed to calculate the k_{eff} bias and k_{eff} bias uncertainty using the bias ($\overline{X_i}$) and bias uncertainty (σ_i). Equation (7) calculates the perturbed ND, which is used to determine the k_{eff} bias and k_{eff} bias uncertainty. The basis ND, as detailed in Tables 11 and is derived from a previous study [46].

$$c_i = c_{i,basis} \cdot \left(\overline{X}_i + \sigma_i \cdot R^k\big|_{normal}\right) \tag{7}$$

where c_i is the *i*th isotopic composition; *i* is the isotopic index; and $c_{i,basis}$ is the reference isotopic composition. The reference isotope composition is presented in Table 11, and was obtained from the CB6 document [46], where *R* is a random number, $R^k|_{normal}$ is the random number that follows the normal distribution, *k* is the index of the random seed, $\overline{X}_i$ is the mean of the isotope composition, and σ_i is the uncertainty of the isotope composition. A total of 250 perturbed isotope compositions were used to calculate the k_{eff} bias and k_{eff} bias uncertainty. The number 250 was selected to satisfy the under 0.00050 standard deviation of the Monte Carlo calculation [14,33].

Table 12 lists the k_{eff} bias and k_{eff} bias uncertainty due to the perturbed isotope compositions using Equation (2). Calculated k_{eff} bias was −0.00666. Compared to previous burnup credit studies [33,48], the calculated k_{eff} bias exhibited a similar trend. Shapiro-Wilk test was used to assess whether distribution shape of calculated 250 multiplication factors follows the normal distribution [25,49]. The calculated values followed a normal distribution (*i.e.*, p-value >0.05). The $\beta_i + \Delta k_i$ is the summation of k_{eff} bias and k_{eff} bias uncertainty due to the isotope composition bias ($\overline{X_i}$) and bias uncertainty (σ_i). Equation (8) was used to calculate $\beta_i + \Delta k_i$, due to the $k_{eff,ref}$ is larger than mean of k_{eff} (*i.e.,* calculated k_{eff} bias is minus value) [14].

$$\beta_i + \Delta k_i = \left(\overline{k_{eff}} - k_{eff,ref}\right) + \sigma_{keff} \times tf_1^{N_C} \tag{8}$$

where β_i is k_{eff} bias, Δk_i is the k_{eff} bias uncertainty, and σ_{keff} is the standard deviation of k_{eff}. $k_{eff,ref}$ was calculated k_{eff} with reference isotope composition presented in the CB6 specification. tf_1 is the single-sided tolerance limit value, and 95 % probability and 95 % confidence level values were used for the calculation. For 250 samples, tf_1 was set to 1.438. These values were obtained from a previous study [50]. The $\sigma_{keff} \times tf_1^{N_C}$ is calculated as 0.01030 (*i.e.,* 0.00716 of σ_{keff} multiplied by tf_1 of 1.438). To determine the bias of the multiplication factor and $\sigma_{keff} \times tf_1^{N_C}$, $\beta_i + \Delta k_i$ was calculated as 0.01696. This value was used to establish the USL for the safety analysis, as shown in Equation (6). The calculated result could be used for novel cask design progress as a criterion of safety analysis [40].

6. Conclusion

A SNF analysis module was developed and incorporated into our in-house nodal diffusion code, RAST-V, to manage the back-end cycle. To

Table 12
k_{eff} bias and k_{eff} bias uncertainty.

Parameter	p-value	k_{eff} bias (β_i)	$\beta_i + \Delta k_i$
Value	0.42129	−0.00666	0.01696

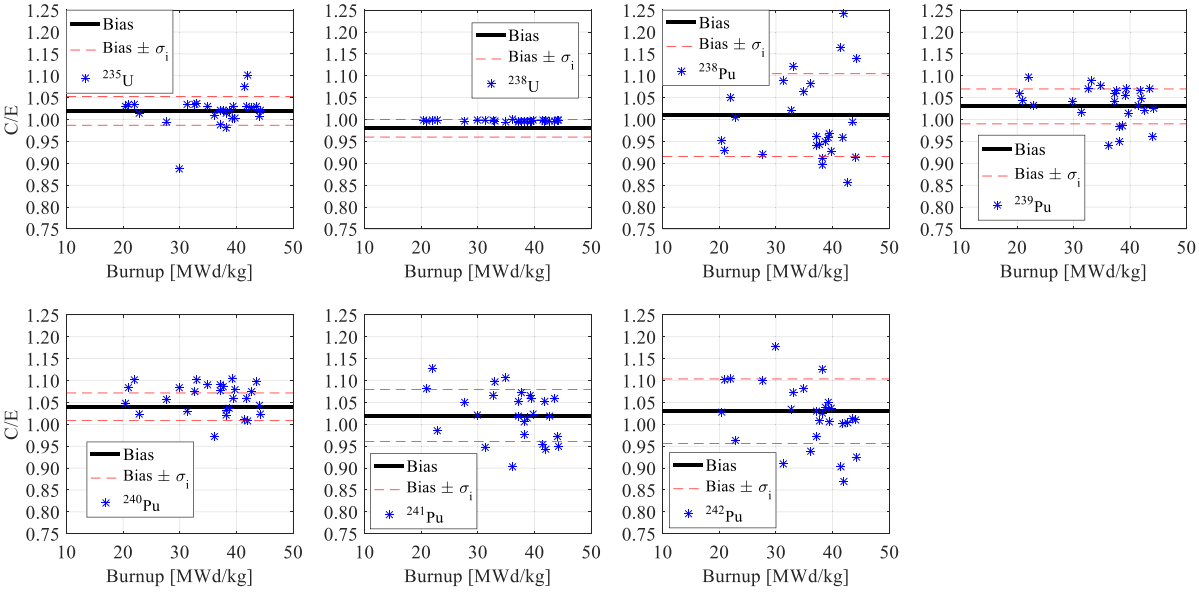

Fig. 21. Bias and bias uncertainty.

broaden the scope of application, the VVER SNF analysis module was implemented using the same code, RAST-V. To evaluate the computational capabilities of the RAST-V SNF, Verification & Validation (V&V) processes were performed using the Novovoronezh-4 nuclear power plant (NPP) Unit 4 and X2 benchmarks.

A total of 28 measurements from Novovoronezh NPP 4 were used for the V&V process. Most of the isotopes showed ±10 % relative differences. Isotopes ^{245}Cm and ^{246}Cm exhibited larger differences compared to the others (~50 %), which can be attributed to three main reasons: the neighboring effect (~20 %), uncertainty due to neutronics data (~20 %), and uncertainty due to the standard deviation of the burnup indicator (~5 %).

In total, 182 fuel assemblies (FAs) (91 once-burned FAs and 91 twice-burned fuels) were used for comparison. In this comparison, RAST-V was found to be 10^5 times faster than STREAM, reducing the re-depletion calculation time while achieving ±10 % difference for most isotopes. The generation of ND files accounted for the majority of the simulation time. Although the generation of these files was time-consuming, RAST-V exhibited an advantage in terms of simulation time, as a finite number of FAs were loaded into the core.

As a part of this application, burnup credit calculations are performed using the CB1, CB3, and CB6 benchmarks. To maximize economic benefits, a burnup credit approach was suggested. This approach provides less conservative criteria for using SNFs instead of fresh fuel to establish an upper safety limit (USL). Nineteen isotopes from 23 samples were used to define the k_{eff} bias and k_{eff} bias uncertainty, using the cask model described in the CB6 benchmark. A Monte Carlo code, Serpent 2, was used for cask analysis, and the cask model demonstrated a difference of −3 pcm compared to previous studies. A total of 250 perturbed ND sets were utilized to calculate the k_{eff} bias and k_{eff} bias caused by the isotope composition, following the NUREG/CR-7108 document approach. The calculated k_{eff} bias and k_{eff} bias were 0.01696, indicating reliability in the burnup range of 20.4–46.3 MWd/kg.

This study successfully outlined the computational features for SNF analysis with V&Vs and provided a sample application calculation with an established k_{eff} bias and k_{eff} bias uncertainty for the USL. A limitation of the current burnup credit calculation is the relatively small number of samples, resulting in narrow burnup range coverage. To address this issue, future studies will involve burnup credit calculations using more samples. Furthermore, the validation process was improved by considering the neighboring FAs effect in the analysis of Novovoronezh-4 samples.

Declaration of competing interest

The authors declare that they have no known competing financial interests or personal relationships that could have appeared to influence the work reported in this paper.

Acknowledgments

This work was supported by the National Research Foundation of Korea (NRF) grant funded by the Korea government (MSIT). (No. NRF-2019M2D2A1A03058371).

Abbreviations

3D	three-dimensional
BOR	boron concentration
CBC	critical boron concentration
CMFD	coarse mesh finite difference
CR	control rod
CRAM	Chebyshev rational approximation method
FA	fuel assembly
ND	number density
NPP	nuclear power plant
PSM	pin-based slowing-down method
PWR	pressurized water reactor
RMS	root mean square
RV	RAST-K VVER
ST	STREAM
SNF	spent nuclear fuel
TFU	fuel temperature
TH	thermal-hydraulic
TH1D	one-dimensional thermal-hydraulic feedback
TPEN	Triangular-based polynomial expansion nodal method
TMO	moderator temperature
USL	upper safety limit
VVER	Vodo-Vodyanoi Energetichesky Reactor
V&V	verification and validation
XS	cross section
XSFB	cross section feedback

References

[1] J. Jang, B. Ebiwonjumi, W. Kim, J. Park, J. Choe, D. Lee, Validation of spent nuclear fuel decay heat calculation by a two-step method, Nucl. Eng. Technol. 53 (2021) 44–60, https://doi.org/10.1016/j.net.2020.06.028.

[2] J. Jang, B. Ebiwonjumi, W. Kim, A. Cherezov, J. Park, D. Lee, Verification and validation of isotope inventory prediction for back-end cycle management using two-step method, Nucl. Eng. Technol. 53 (2021) 2104–2125, https://doi.org/10.1016/j.net.2021.01.009.

[3] J. Park, J. Jang, H. Kim, J. Choe, D. Yun, P. Zhang, A. Cherezov, D. Lee, RAST-K v2—three-dimensional nodal diffusion code for pressurized water reactor core analysis, Energies 13 (2020) 6324, https://doi.org/10.3390/en13236324.

[4] Current Status of World Nuclear Fuel Cycle Technology (III): Russia and Soviet Union, KAERI/AR-826/2008, KAERI, 2008. https://inis.iaea.org/collection/NCLCollectionStore/_Public/41/067/41067574.pdf.

[5] The VVER today, ROSATOM. https://rosatom.ru/upload/iblock/0be/0be1220af25741375138ecd1afb18743.pdf. Accessed May 31.

[6] L.J. Jardine, Radiochemical Assays of Irradiated VVER-440 Fuel for Use in Spent Fuel Burnup Credit Activities, UCRL-TR-212202, Lawrence Livermore National Laboratory, 2005.

[7] Y. Bilodid, E. Fridman, T. Lötsch, X2 VVER-1000 benchmark revision: fresh HZP core state and the reference Monte Carlo solution, Ann. Nucl. Energy 144 (2020), https://doi.org/10.1016/j.anucene.2020.107558.

[8] J. Jang, S. Dzianisau, D. Lee, Development of nodal diffusion code RAST-V for Vodo–Vodyanoi Energetichesky reactor analysis, Nucl. Eng. Technol. 54 (2022) 3494–3515, https://doi.org/10.1016/j.net.2022.04.007.

[9] Online, Power reactor information system. https://pris.iaea.org/PRIS/CountryStatistics/ReactorDetails.aspx?current=448, International Arts and Entertainment Alliance.

[10] Online, Novovoronezh Unit 4 Completes Upgrade, World nuclear news, 2018. https://world-nuclear-news.org/Articles/Novovoronezh-unit-4-completes-upgrade.

[11] L. Markova, Continuation of the VVER Burnup Credit Benchmark: Evaluation of CB1 Results, Overview of CB2 Results to Date and Specification of CB3, 8th Symposium AER, Bystrice n. Pernstejnem, 1998. https://inis.iaea.org/collection/NCLCollectionStore/_Public/32/068/32068921.pdf.

[12] L. Markova, Specification for CB 6 Benchmark on VVER-440 Final Disposal, 2010. https://www.oecd-nea.org/science/wpncs/buc/specifications/CB6-VVER-Disposal-benchmark.pdf.

[13] B. Ebiwonjumi, S. Choi, M. Lemaire, D. Lee, H.C. Shin, Validation of lattice physics code Stream for predicting pressurized water reactor spent nuclear fuel isotopic inventory, Ann. Nucl. Energy 120 (2018) 431–449, https://doi.org/10.1016/j.anucene.2018.06.002.

[14] G.I. Radulescu, C.G. Gauld, J. Llas, C. Wagner, NUREG/CR-7108 an Approach for Validating Actinide and Fission Product Burnup Credit Criticality Safety Analyses—Isotopic Composition Predictions, Oak Ridge National Laboratory, April 2012.

[15] M. J, D. Scaglione, E.J. Mueller, C.W. Wagner, J. Marshall, NUREG/CR-7109, an Approach for Validating Actinide and Fission Product Burnup Credit Criticality Safety Analyses—Criticality (Keff) Predictions, Oak Ridge National Laboratory, April 2012.

[16] User's Guide HDF5 Release 1.10, The HDF Group, 2019. https://portal.hdfgroup.org/display/HDF5/HDF5+User+Guides?preview=/53610087/53610088/Users_Guide.pdf.

[17] B. Vrban, J. Lüley, Š. Čerba, F. Osuský, V. Nečas, The VVER-440 Burnup Credit Computational Benchmark Used for the SCALE System Qualification, Applied Physics of Condensed Matter, APCOM 2018, 2018.

[18] A. Ranta-aho, Validation of Depletion Codes against VVER-440 Spent Fuel Data, vol. 31, NEA/NSC/DOC(2006, Prague, Czech Republic, 2006. https://www.oecd.org/officialdocuments/publicdisplaydocumentpdf/?cote=NEA/NSC/DOC(2006)31&docLanguage=En.

[19] J. Jang, Y. Chezerov, T. Jo, S. Quoc, W. Dzianisau, J. Lee, D. Park, Lee, Verification of RAST-K Hexagonal Transient Solver with OCED/NEA Benchmark Problem of KALININ-3 NPP, KNS Winter Meeting, Korea, 2020. Online.
[20] S. Quoc, W. Dzianisau, D. Lee, J. Lee, T. Jang T, Verification of RAST-K Hexagonal Analysis Module with SNR and VVER-440 Benchmarks, KNS Winter Meeting, Korea, 2020 [Online].
[21] J. Jang, M. Hursin, W. Lee, A. Pautz, M. Papadionysiou, H. Ferroukhi, D. Lee, Analysis of Rostov-II benchmark using conventional two-step code systems, Energies 15 (2022) 3318, https://doi.org/10.3390/en15093318.
[22] J. Jang, Development of Nodal Diffusion Code for VVER and HTGR Analysis with Advanced Semi Analytic Nodal Method, Doctoral Thesis, Ulsan National Institute of Science and Technology, 2023.
[23] J.Y. Cho, C.H. Kim, Higher order polynomial expansion nodal method for hexagonal core neutronics analysis, Ann. Nucl. Energy 25 (1998) 1021–1031, https://doi.org/10.1016/S0306-4549(97)00101-1.
[24] S. Choi, W. Kim, J. Choe, W. Lee, H. Kim, B. Ebiwonjumi, E. Jeong, K. Kim, D. Yun, H. Lee, D. Lee, Development of high-fidelity neutron transport code STREAM, Comput. Phys. Commun. 264 (2021) 107915, https://doi.org/10.1016/j.cpc.2021.107915.
[25] A. Quarteroni, R. Sacco, F. Saleri. Numerical Mathematics, 2nd ed., Springer, 2007, ISBN 978-1-4757-7394-1 https://doi.org/10.1007/b98885.
[26] R.J.J. Stamm'ler, M.J. Abbate, Methods of Steady-State Reactor Physics in Nuclear Design, Academic Press Inc. (LONDON) LTD, 1983, 0-12-663320-7.
[27] S. Børresen, T. Bahadir, M. Kruners, Validation of CMS/SNF Calculations against Preliminary CLAB Decay Heat Measurements, Transactions of the American nuclear society, Omni Shoreham Hotel Washington, D.C., 2004. November 14-18.
[28] S. Børresen, Spent fuel analyses based on in-core fuel management calculations, in: Proc. PHYSOR (2004). The Physics of Fuel Cycles and Advanced Nuclear Systems, Global Developments, Chicago, Illinois, 2004. April 25-29.
[29] bib29sref29 Markova, L., Simplified benchmark specif. Based on vol. 2670 ISTC VVER PIE. 12th Meeting of AER Working Group E on "Physical Problems of Spent Fuel, Radwaste and Nuclear Power Plants Decommissioning", Modra, Slovakia, April 16-18, 2007, https://www.oecd-nea.org/science/wpncs/buc/specifications/istc2670/2670%20benchmark%20specification.pdf.
[30] F. Michel-Sendis, I. Gauld, J.S. Martinez, C. Alejano, M. Bossant, D. Boulanger, O. Cabellos, V. Chrapciak, J. Conde, I. Fast, M. Gren, K. Govers, M. Gysemans, V. Hannstein, F. Havlůj, M. Hennebach, G. Hordosy, G. Ilas, R. Kilger, R. Mills, D. Mountford, P. Ortego, G. Radulescu, M. Rahimi, A. Ranta-Aho, K. Rantamäki, B. Ruprecht, N. Soppera, M. Stuke, K. Suyama, S. Tittelbach, C. Tore, S.V. Winckel, A. Vasiliev, T. Watanabe, T. Yamamoto, T. Yamamoto, SFCOMPO-2.0: an OECD NEA database of spent nuclear fuel isotopic assays, reactor design specifications, and operating data, Ann. Nucl. Energy 110 (2017) 779–788, https://doi.org/10.1016/j.anucene.2017.07.022.s.
[31] M.B. Chadwick, P. Obložinský, M. Herman, N.M. Greene, R.D. McKnight, D. L. Smith, P.G. Young, R.E. MacFarlane, G.M. Hale, S.C. Frankle, A.C. Kahler, T. Kawano, R.C. Little, D.G. Madland, P. Moller, R.D. Mosteller, P.R. Page, P. Talou, H. Trellue, M.C. White, W.B. Wilson, R. Arcilla, C.L. Dunford, S.F. Mughabghab, B. Pritychenko, D. Rochman, A.A. Sonzogni, C.R. Lubitz, T.H. Trumbull, J. P. Weinman, D.A. Brown, D.E. Cullen, D.P. Heinrichs, D.P. McNabb, H. Derrien, M. E. Dunn, N.M. Larson, L.C. Leal, A.D. Carlson, R.C. Block, J.B. Briggs, E.T. Cheng, H.C. Huria, M.L. Zerkle, K.S. Kozier, A. Courcelle, V. Pronyaev, S.C. van der Marck, ENDF/B-VII.0: next generation evaluated nuclear data library for nuclear science and technology, Nucl. Data Sheets, ENDF/B. 107 (2006) 2931–3060, https://doi.org/10.1016/j.nds.2006.11.001.
[32] O. Leray, D. Rochman, P. Grimm, H. Ferroukhi, A. Vasiliev, M. Hursin, G. Perret, A. Pautz, Nuclear data uncertainty propagation on spent fuel nuclide compositions, Ann. Nucl. Energy 94 (2016) 603–611, https://doi.org/10.1016/j.anucene.2016.03.023.
[33] J. Jang, C. Kong, B. Ebiwonjumi, Y. Jo, D. Lee, Uncertainties of PWR spent nuclear fuel isotope inventory for back-end cycle analysis with Stream/RAST-K, Ann. Nucl. Energy 158 (2021), https://doi.org/10.1016/j.anucene.2021.108267.
[34] Techniques and equipment to determine nuclide composition, Isotopic Mass and Fuel Burnup Fraction in Fuel Samples. Interim Progress Report, Task 6, Burnup Credit Project, 2003, p. 2670p.
[35] ASTM E-244-80, Standard Test Method for Atom Percent Fission in Uranium and Plutonium Fuel (Mass Spectrometric Method).
[36] MATLAB, The MathWorks Incorp, Natick, Massachusetts, 2022.
[37] J. Jang, C. Kong, B. Ebiwonjumi, A. Cherezov, Y. Jo, D. Lee, Uncertainty quantification in decay heat calculation of spent nuclear fuel by STREAM/RAST-K, Nucl. Eng. Technol. 53 (2021) 2803–2815, https://doi.org/10.1016/j.net.2021.03.010.
[38] B. Ebiwonjumi, S. Choi, M. Lemaire, D. Lee, H.C. Shin, H.S. Lee, Verification and validation of radiation source term capabilities in Stream, Ann. Nucl. Energy 124 (2019) 80–87, https://doi.org/10.1016/j.anucene.2018.09.034.
[39] T.S. Lötsch, E. Kliem, V. Bilodid, A. Khalimonchuk, Y. Kuchin, M. Ovdienko, R. Ieremenko, G. Blank, Schultz, The x2 benchmark for vver-1000 reactor calculations results and status, in: Novel Vision of Scientific & Technical Support for Regulation of Nuclear Energy Safety: Competence, Transparency, Responsibility, Dedicated to the 25th Anniversary of the SSTC, National Rosacea Society, Kiev, Ukraine, 2017. March 22–23.
[40] M. Rezaeian, J. Kamali, Effect of a dual-purpose cask payload increment of spent fuel assemblies from VVER 1000 Bushehr Nuclear Power Plant on basket criticality, Appl. Radiat. Isot. 119 (2017) 80–85, https://doi.org/10.1016/j.apradiso.2016.10.008.
[41] J. Leppänen, M. Pusa, T. Viitanen, V. Valtavirta, T. Kaltiaisenaho, The Serpent Monte Carlo code: status development and applications in 2013, Ann. Nucl. Energy 82 (2015) 142–150, https://doi.org/10.1016/j.anucene.2014.08.024.
[42] S. Choi, W. Kim, J. Choe, W. Lee, H. Kim, B. Ebiwonjumi, E. Jeong, H. Lee, D. Yun, D. Lee, Development of high-fidelity neutron transport code STREAM, Comput. Phys. Commun. 264 (2021), 107915, https://doi.org/10.1016/j.cpc.2021.107915.
[43] S. Choi, K. Smith, H. Chul Lee, D. Lee, Impact of inflow transport approximation on light water reactor analysis, J. Comput. Phys. 299 (2015) 352–373, https://doi.org/10.1016/j.jcp.2015.07.005.
[44] H. Yun, K. Park, W. Choi, S.G. Hong, An efficient evaluation of depletion uncertainty for a GBC-32 dry storage cask with PLUS7 fuel assemblies using the Monte Carlo sampling method, Ann. Nucl. Energy 110 (2017) 679–691.
[45] S. Choi, H. Lee, S.G. Hong, D. Lee, Resonance self-shielding methodology of new neutron transport code STREAM, J. Nucl. Sci. Technol. 52 (9) (2015) 1133–1150, https://doi.org/10.1080/00223131.2014.993738.
[46] T. Lahtinen, Solution of the CB6 benchmark on VVER-440 final disposal using the Serpent reactor physics code, Kerntechnik 79 (2014) 303–313, https://doi.org/10.3139/124.110464.
[47] Thermal Neutron Capture Cross Sections Resonance Integrals and G-Factors, S.F. Mughabghab, Brookhaven National Laboratory, Upton, New York, U.S.A, 2003, pp. 11973–15000. https://www.osti.gov/etdeweb/servlets/purl/20332542. February.
[48] I.C. Gauld, U. Mertyurek, C. I, U. Gauld, Mertyurek, alidation of BWR spent nuclear fuel isotopic predictions with applications to burnup credit, Nucl. Eng. Des. 345 (2019) 110–124, https://doi.org/10.1016/j.nucengdes.2019.01.026.
[49] R. Ihaka, R. Gentleman, R: a language for data analysis and graphics, J. Comput. Graph Stat. 5 (1995) 299–314, https://doi.org/10.2307/1390807.
[50] W.R. Blischke, D.N. Prabhakar Murthy, Reliability: Modeling, Prediction, and Optimization, Wiley, 2000, 9780471184508.